Elasticity of Calcium and Calcium-Sodium Amphiboles

J. Michael Brown* brown@ess.washington.edu
Fax: 206 543 0489

Evan H. Abramson evan@ess.washington.edu

Earth and Space Sciences
University of Washington
Seattle, WA 98195-1310

*Corresponding author

Abstract

Measurements of single-crystal elastic moduli under ambient conditions are reported for nine calcium to calcium-sodium amphiboles that lie in the composition range of common crustal constituents. Velocities of body and surface acoustic waves measured by Impulsive Stimulated Light Scattering (ISLS) were inverted to determine the 13 moduli characterizing these monoclinic samples. Moduli show a consistent pattern: $C_{33}>C_{22}>C_{11}$ and $C_{23}>C_{12}>C_{13}$ and $C_{44}>C_{55}\sim C_{66}$ and for the uniquely monoclinic moduli, $|C_{35}|>>C_{46}\sim|C_{25}|>|C_{15}|\sim 0$. Most of the compositionally-induced variance of moduli is associated with aluminum and iron content. Seven moduli (C_{11} C_{12} C_{13} C_{22} C_{44} C_{55} C_{66}) increase with increasing aluminum while all diagonal moduli decrease with increasing iron. Three moduli (C_{11}, C_{13} and C_{44}) increase with increasing sodium and potassium occupancy in A-sites. The uniquely monoclinic moduli (C_{15} C_{25} and C_{35}) have no significant compositional dependence. Moduli associated with the a^* direction (C_{11} C_{12} C_{13} C_{55} *and* C_{66}) are substantially smaller than values associated with structurally and chemically related clinopyroxenes. Other moduli are more similar for both inosilicates. The isotropically averaged adiabatic bulk modulus does not vary with iron content but increases with aluminum content from 85 GPa for tremolite to 99 GPa for pargasite. Increasing iron reduces while increasing aluminum increases the isotropic shear modulus which ranges from 47 GPa for ferro-actinolite to 64 GPa for pargasite. These results exhibit far greater anisotropy and higher velocities than apparent in earlier work. Quasi-longitudinal velocities are as fast as ~9 km/s and (intermediate between the a^*- and c-axes) are as slow as ~6 km/s. Voigt-Reuss-Hill averaging based on prior single crystal moduli resulted in calculated rock velocities lower than laboratory measurements, leading to adoption of the (higher velocity) Voigt bound. Thus, former uses of the upper Voigt bound can be understood as an *ad hoc* decision that compensated for inaccurate data. Furthermore, because properties of the end-member amphiboles deviate substantially from prior estimates, all predictions of rock velocities as a function of modal mineralogy and elemental partitioning require reconsideration.

Key Words: elasticity; anisotropy; seismic velocities; aggregate elasticity; amphibole; hornblende

1. Introduction

Amphiboles are abundant in crustal igneous and metamorphic rocks. They exhibit a wide range of compositions as a result of extensive solid solution behavior, accommodating all of the abundant cation species (silicon, aluminum, magnesium, iron, calcium, sodium, and potassium). The structure also contains ~2 wt% bound water. When subducted, dehydration reactions in rocks containing amphiboles release water at depth that probably affects the evolution of magma in arc volcanism and is likely associated with intermediate and deep earthquakes (Hacker *et al.* 2003a) as well as seismic tremor/slow slip (Audet et al., 2010).

Since amphiboles are ubiquitous, the description of the crustal seismic structure requires characterization of their elastic properties (*e.g.* Christensen and Mooney 1995, Christensen 1996, Hacker *et al.* 2003b, Barberini *et al.* 2007, Tatham *et al.* 2008, Llana-Funez and Brown 2012, Ji *et al.* 2013, Selway *et al.* 2015). However, knowledge concerning their single-crystal elasticity and compositional dependences has remained elusive. In the pioneering work that continues to be cited, Aleksandrov and Ryzhova (1961a) reported single crystal elastic moduli for two "hornblendes" of unspecified composition based on only slightly over-determined sets of ultrasonic velocity measurements on megacrysts under ambient conditions. As previously demonstrated in studies of feldspars (Brown *et al.* 2006; Brown *et al.* 2016; and Waeselmann *et al.* 2016), results from these early studies have proven to be systematically in error.

That the early ultrasonic results under-estimate velocities most likely was a result of open cleavage surfaces and cracks. Also contributing was an inadequate sampling of velocities as a function of propagation direction. Based on the lack of reported chemistry and probable systematic errors, these early results are considered here in the context of having incorrectly influenced various interpretations of crustal seismic structure that were grounded on mineral properties. In particular, in order to better match laboratory measurements, the compensating use of the upper Voigt bound when calculating aggregate rock velocities has been common. In contrast, Watt and O'Connell (1980) demonstrated that, in well-characterized and nearly crack-free samples, velocities in two phase aggregates fell within the Hashin-Shtrikman bounds which lie between the extremal Voigt and Reuss bounds (see also Watt *et al.* 1976).

A few determinations of single-crystal elastic properties are available within the broad range of amphibole compositions. Bezacier *et al.* (2010) gave elastic moduli for a crystal having a composition near the glaucophane end-member. High pressure x-ray cell parameter determinations have been reported for tremolite, pargasite, and glaucophane (Comodi *et al.* 1991) and for synthetic glaucophane (Jenkins *et al.* 2010).

Hacker *et al.* (2003b) compiled available (isotropically averaged) elasticity data for important rock-forming minerals including amphiboles. They excluded the Aleksandrov and Ryzhova (1961a) moduli as probably being in error and relied on the Christensen (1996) rock velocity measurements to estimate properties of an average crustal "hornblende". To constrain properties of other end-member

compositions, they used bulk moduli from the Holland and Powell (1998) thermodynamic database plus the Comodi *et al.* (1991) compression measurements. Although an isothermal bulk modulus can be inferred from pressure-induced strains, the shear modulus, necessary to estimate body wave velocities, cannot be determined solely from the hydrostatic x-ray data. Instead, Hacker *et al.* (2003b) estimated shear moduli on the basis of the reported bulk moduli and an assumed Poisson's ratio. They noted that this was a remaining source of uncertainty.

As noted in section 6.3, an isothermal bulk modulus measured under hydrostatic compression (which is equivalent to the elastic aggregate lower-bound Reuss average) is significantly smaller than the appropriate Voigt-Reuss-Hill or Hashin-Shtrikman bulk modulus used for calculation of seismic velocities. Bulk moduli for some amphiboles given by Hacker *et al.* (2003b) appear to represent the Reuss bound. They combined lower bound moduli (in some cases) in an upper-bound Voigt average for calculations of velocities in rocks as mixtures of minerals. Thus, the accuracy of their analysis relied on how well the two errors off-set each other.

Here elastic moduli are reported for nine amphiboles that lie in the range of compositions commonly found in crustal rocks (Schumacher 2007). Elastic wave velocities (quasi-longitudinal, quasi-transverse and surface acoustic waves - SAW) were measured using Impulsive Stimulated Light Scattering (ISLS) (Abramson *et al.* 1999). A joint inversion allowed accurate determination of the 13 elastic moduli for these monoclinic minerals. The dependences of moduli on composition are determined through linear regression. From these, relationships to crystal structure and seismic velocities can be explored. Ultimately, more accurate predictions of seismic properties of rocks can be undertaken on the basis of modal mineralogy and elemental partitioning.

2. Amphibole chemistry and structure

As reviewed by Hawthorn and Oberti (2007), the monoclinic (*C2/m*) calcium (including common hornblende) to calcium-sodium amphiboles have a generalized formula of

$$A_{0\text{-}1}B_2C_5T_8O_{22}\,(OH)_2$$

where the A-site is occupied by sodium and potassium or remains vacant and the B-site is occupied by sodium or calcium. The octahedrally coordinated C-sites contain iron (divalent or trivalent), magnesium, or aluminum (designated as ^{vi}Al). The tetrahedral T-sites contain silicon and aluminum (typically up to two aluminum per eight sites, occasionally more, and designated as ^{iv}Al). Other common minor chemical components (Ti, Mn, Co, Cr) are found in size and valence-state appropriate sites. Fluorine and chlorine can substitute for OH^{-1}.

Figure 1

The naming conventions associated with chemistry of calcium and sodium amphiboles (Hawthorne *et al.* 2012, see also Leake *et al.* 1997) are illustrated in Figure 1 using three compositional variables. Although complete solid-solution substitution is possible within this compositional space, several of the stoichiometric compositions are given discrete names. Tremolite is $[]Ca_2Mg_5Si_8O_{22}(OH)_2$ (where the brackets denote the vacant A-site) while winchite

has one calcium and one sodium in the B-site. Glaucophane has all sodium in the B-site with coupled substitutions of a trivalent cation in C-sites required to balance charge. Hornblende is both an end-member in Figure 1 and is a generalized term for calcium amphiboles with intermediate tetrahedral aluminum compositions. In addition, solid-solution substitution of iron for magnesium gives rise to iron end-members for all phases shown in Figure 1 with ferro- added to the name (*e.g.* ferro-pargasite).

Amphiboles have I-beam structures of two double tetrahedral chains that are bonded to each other by an octahedral sheet containing five C-site cations. The I-beams are oriented along the *c*-axis with A-site cations (when present) bonding the I-beams along the *a*-axis and B-site cations serving to bond I-beams along the *b*-direction. Clinopyroxenes share similar chemical variations in a structure that is closely related to the amphiboles, both being inosilicates but the pyroxenes have a single tetrahedral chains aligned along the *c*-axis. The general formula of the clinopyroxene is BCT_2O_6 with the B and C sites being equivalent to those found in the amphiboles. End member pyroxenes include diopside ($CaMgSi_2O_6$) hedenbergite ($CaFeSi_2O_6$), and jadeite ($NaAlSi_2O_6$).

Having a wide range of solid-solution substitutions for essentially the same crystal structure, amphiboles provide a natural laboratory for the exploration of chemical controls on elasticity. Variations in elastic moduli are anticipated from changes of ionic sizes and charges, as a result of cation substitutions in the A, B, C and T sites. Comparisons of elasticity between pyroxenes and amphiboles provides further opportunities to explore factors influencing elastic behavior.

3. Sample sources and characterization

The sources, localities (when known), x-ray determined cell parameters, and densities of nine amphiboles are given in Table 1. Individual crystals as 2-3 mm mineral separates were obtained either from disaggregated crystalline rocks or were broken off larger previously collected crystals. Chemical homogeneity of samples from each source was confirmed by application of analytic methods to all individual samples used in the study.

Table 1

Table 2

Microprobe analyses for all samples are reported in Table S1 of the supporting materials. A lack of chemical zoning was confirmed in all crystals and the reported analyses are the averages of point determinations across each crystal. Structural formula, based on Probe-AMPH (Tindle and Webb, 1994), are given in Table 2 and are plotted in perspective in Figure 1. Samples 1 and 2 with ~1 sodium in the B-site are classified as calcium-sodium amphiboles. The remaining seven samples are calcium amphiboles. The chemistry of the glaucophane sample used by Bezacier *et al.* (2010) and the average calcium amphibole composition reported by Schumacher (2007) are also included in Table 2. As noted by Schumacher (2007), calcium amphiboles cover a wide range of intermediate compositions within the compositional space defined in Figure 1 and his reported average (based on over 1700 published analyses) may be a biased estimator of an average "hornblende" in crustal rocks since samples were analyzed for specific science interests rather than being chosen to best represent crustal chemistry. Nonetheless, this average

Figure 2

provides a reference point, defining a common hornblende composition in the following discussion.

The nine samples used in this study show a range of compositions (Figure 2) that generally brackets the averages reported by Schumacher (2007). This is prerequisite to determining compositional contributions to the elastic properties within the appropriate bounds of elemental partitioning in crustal calcium amphiboles.

4. Experimental methods

The following convention is adopted to align the crystallographic axes with respect to the Cartesian axes for the description of the elastic tensor. The Y axis is aligned parallel to the crystallographic *b*-axis and the Z axis is aligned parallel to the *c*-axis. The X axis is set in the a^*-direction (perpendicular to the *b*- and *c*-axes). Elastic moduli (stiffnesses) are represented by the 6 by 6 matrix C_{ij} using the Voigt convention. The inverse of this matrix is the compliance matrix S_{ij}.

The vertical sum of the first three rows of the compliance matrix gives six strains, β_i, associated with the application of unit hydrostatic stress. Based on 2/m symmetry β_4 and β_6 are zero. These strains can be cast as a 3x3 symmetric tensor which gives crystal compressibility under hydrostatic stress at the limit of zero stress.

Three crystals for each sample were oriented on an x-ray diffractometer. The crystals, in selected crystallographic orientations, were glued to glass slides (mechanically indexed to laboratory coordinates) while still attached to the x-ray goniometer head. Samples were subsequently ground and polished on two sides using ¼ micron diamond grit for the final polish. The final thicknesses of samples were over an order of magnitude greater than the nominal acoustic wavelength (~ 2.5 microns). The orientations of several samples, re-checked on the x-ray diffractometer after completion of the grinding and polishing process, agreed with the original orientation to within four degrees. Prior to measurements of SAW velocities, a 40 (+/-5) nm layer of aluminum was deposited on the top polished surface. This metallic layer allowed coupling of the incident laser energy to the sample surface (Brown *et al.* 2006). The change in velocity caused by the aluminum layer is less than 0.2% and is accounted for in the analysis described below.

Both body wave (quasi-longitudinal and quasi-transverse) and surface acoustic wave (SAW) velocities were measured using the method of Impulsive Stimulated Light Scattering (ISLS) (Abramson *et al.* 1999). The excitation spot size was about 200 microns and the probe was focused to about 15 microns. Since optical absorption is small in these samples, laser heating is estimated to be less than 0.2°C (Brown *et al.* 1989). In the case of SAW measurements, the excitation laser intensity was reduced well below the power required to damage the surface coating and the heat absorbed by the thin aluminum layer resulted in a negligible changes of sample temperatures.

The optical quality of the natural samples in some cases presented experimental challenges. Optical defects (including cracks, cleavage separations, and inclusions) were common. These served to incoherently scatter the probe laser, causing

saturation of the detector. Successful measurements could be made if a ~100 micron nearly defect-free region was available. Since polished surfaces were typically greater than 1000 microns across, regions of adequate quality could usually be found. Photomicrographs (supplemental materials Figure S1) of several samples illustrates typical crystal quality for these experiments.

All measurements (typically between 150 and 200 individual velocity determinations per sample) are reported in Table S2 of the supplementary materials. Further details of the experiments and the methods used to determine elastic parameters for low symmetry minerals have been described for body wave measurements (Collins and Brown 1998) and, separately, for SAW measurements (Brown *et al.* 2006). The three euler angles that relate the crystal axes to laboratory coordinates were also optimized to account for the orientation errors introduced by the sample processing steps given in the first paragraph of this section. The numerical methods are described in Brown (2016).

New in this work is the joint inversion of both body and SAW velocities as described in Brown (2016). Although a complete body wave data set is sufficient to determine all elastic moduli, as noted above, it proved difficult to obtain a full set of velocities (quasi-longitudinal and two polarizations of quasi-transverse waves) for all propagation directions. In some directions, internal flaws scattered light so strongly that the body wave signal could not be recovered from the background. Separately, velocities for both polarizations of transverse waves could not always be obtained in an adequate number of propagation directions as a result of small values of either the (angle-dependent) piezo-optic coefficient or absorption. SAW velocities, based on light coherently scattered from a polished surface, could be more readily measured for all directions of propagation.

The typical *rms* misfit (reported in Table S2) obtained through joint fitting of all measurements is ~0.3%. This is 10-12 m/s for SAW (for nominal velocities near 3-4 km/s) and 16-20 m/s for body waves (for nominal velocities of 6-9 km/s for quasi-longitudinal and 3-5 km/s for quasi-transverse waves). Such misfits are essentially identical to those previously reported for individually analyzed body wave and SAW data sets (*e.g.* Collins and Brown 1998 and Brown *et al. 2*016) and are thought to represent intrinsic random errors associated with studies based on natural crystals. Thus, no additional systematic errors appear to have been introduced through joint analysis of body wave and SAW velocities. Furthermore, the consistency of velocities measured in separate crystals with different orientations for similar polarizations and propagation directions and the consistency of results for surface waves that probed the top few microns of each crystal relative to body wave measurements that sampled a larger internal volume, argues that the crystals were adequately homogeneous and that the moduli are representative of each compositional sample.

The resulting elastic moduli C_{ij} and their associated 2σ uncertainties are listed in Table 3 for the nine amphiboles plus glaucophane. The compliance matrix elements S_{ij} (inverse of the matrix C_{ij}) and compliances sums, β_i, are listed in Table S2. The sums are also given in principal axis coordinates of the hydrostatic compressibility ellipsoid.

Table 3

Body wave velocities for glaucophane in Bezacier *et al.* (2010) were reanalyzed using the same numerical optimization methods used here. Optimization of crystal euler angles allowed reduction of velocity misfit from the previously reported *rms* error of 43 m/s (~0.8% scatter in velocity measurements) to 37 m/s (~0.6% velocity scatter). Some of the new moduli differ by ~2 GPa . Some uncertainties given by Bezacier *et al.* (2010) are substantially different from those reported here (see further discussion in Brown 2016). In particular, it would appear that previously reported uncertainties of some off-diagonal moduli were under-estimated and several diagonal uncertainties were over-estimated. Moduli uncertainties for glaucophane are roughly twice as large as those for the calcium and calcium-sodium amphiboles as is appropriate for the observed larger misfit to measured velocities.

5. Elastic moduli and their compositional dependence

Elastic moduli and isotropic body wave velocities are plotted as a function of total aluminum in Figure 3. Also shown are predictions (described below) based on linear regression in chemical composition that account for most of the observed variance. Moduli that are non-zero for orthorhombic crystals are shown in the top three panels. The uniquely monoclinic moduli are plotted in the lower left panel. Adiabatic bulk and shear moduli given as the mean of Hashin-Shtrikman bounds (Brown 2015) are shown in the middle lower panel and the resulting isotropic compressional and transverse wave velocities are in the lower right panel.

Figure 3

For all compositions, the relative sizes of the moduli remain consistent. That is $C_{33}>C_{22}>C_{11}$ and $C_{23}>C_{12}>C_{13}$, and $C_{44}>C_{55}\sim C_{66}$ and for the uniquely monoclinic moduli, $|C_{35}|>>C_{46}\sim|C_{25}|>|C_{15}|\sim 0$. The same pattern and roughly similar moduli are apparent for glaucophane. However, the C_{22}, C_{33}, and C_{23} moduli of glaucophane are significantly stiffer. As further discussed below, the large value of C_{35} (comparable to the off-diagonal orthorhombic moduli and larger than all other monoclinic moduli) is responsible for a rotation of elastic extrema in the crystallographic plane containing the *a*- and *c*-axes.

Six chemical controls on elasticity associated with changes in cation charges and sizes can be identified as likely to produce significant effects. These are (1) total aluminum content, or its separate content in either (2) T-sites or (3) C-sites, (4) iron content in C-sites (mainly replacing magnesium), the (5) degree of A-site occupation, and (6) sodium replacement of calcium in B-sites. Other possibilities that are less likely to have a measureable impact (including replacement of OH^{-1} with Cl^{-1} or F^{-1}, or changes in the ferric-ferrous iron ratio) could not be investigated using the current samples.

Moduli are assumed to be linear in the six compositional metrics identified above. Tremolite is used as the base composition and changing chemical content is given by the formula unit measures listed in Table 2. A standard statistical measure, the F-test (Rencher 2002), determined the significance of the proposed metrics through stepwise addition and removal of terms using MATLAB® function *stepwiselm.* Only three compositional terms were found to have significant impact at the 95% confidence level; these are total aluminum, A-site occupancy, and iron in the C-site.

Despite the difference in charge and ionic radius, the substitution of sodium for calcium in the B- site appears to have negligible impact on moduli. Nor was the fit significantly improved by allowing separate contributions of aluminum in C- and T-sites. At the 95% confidence level, no tested parameterization could reconcile the glaucophane moduli with the calcium and calcium-sodium amphiboles moduli. This suggests that the elasticity of the fully sodium amphibole does not lie on a continuum of linear solid solution behavior. Regressions based on compositional "vectors" that are linear combination of compositional metrics, as suggested by Schumacher (2007), were not successful.

Regression parameters and misfit statistics are listed in Tables 4 and 5. Blanks in the tables indicate no significant contributions for particular terms. For the three moduli showing sensitivity to A-site occupancy, the alternative parameterizations, using only total aluminum and iron content, are listed with concomitant larger misfits. As shown in the tables, most regression misfits are comparable to experimental uncertainty but tend to be slightly larger. However, further reduction of variance by allowing more degrees of freedom (additional compositional metrics or non-linear dependences of moduli with chemistry) is not statistically robust.

Table 4

Table 5

Predictions for moduli and isotropic velocities based on the three compositional metrics listed in Tables 4 and 5 are represented in Figure 3. Since sample chemistries are variable, predicted moduli and velocities do not, in general, lie on the plotted lines that are based on either iron-free or ferro-equivalent minerals (both with no A-site occupation). In all panels predicted moduli and velocities are nearly within uncertainties of the measurements.

All diagonal elastic moduli (and the isotropic average shear modulus) decrease with the addition of iron and derivatives of these moduli with respect to iron are similar. Seven of thirteen moduli (C_{11} C_{22} C_{13} C_{12} C_{44} C_{55} C_{66}) increase with aluminum content while C_{46} decreases with aluminum. Five moduli (C_{33} C_{23} and the monoclinic moduli C_{15} C_{25} and C_{35}) have no significant dependence on aluminum. Both isotropic moduli (bulk modulus and shear modulus) increase with added aluminum. Only C_{11} C_{13} and C_{44} are dependent on A-site occupancy; misfits are substantially larger for the alternative assumption of no dependence on A-site occupancy. All three compositional metrics are necessary to adequately predict the variations of density and the isotropic transverse wave velocities while aluminum and iron content are sufficient to predict compressional velocities.

6. Discussion

6.1 Compositional and structural controls on elasticity

In Table 6 the elastic moduli of several amphibole compositions are compared with chemically related clinopyroxene. Amphibole moduli associated with longitudinal stresses and strains involving the a^*-axis (*ie.* C_{11} C_{12} C_{13} C_{55} C_{66}) are all significantly smaller than corresponding clinopyroxene moduli by approximately a factor of two while moduli associated with the b- and c-axes (C_{22} C_{33} C_{23} C_{44}) are notably similar. That (as shown in Table 4) C_{11} and C_{13} increase with increasing A-site occupation seems reasonable since cations in the A-site provide additional bonding and thus additional resistance to compression along the a^*-direction. However, even with full

Table 6

A-site occupations, these amphibole moduli remain smaller than those for pyroxenes (that lack the A-site). The reversal of sign for the uniquely monoclinic moduli (C_{15} C_{25} and most importantly C_{35}) are responsible for a major shift in the orientation of anisotropy between amphiboles and pyroxenes that is further discussed in Section 6.2. With a few exceptions, amphiboles and the compositionally related clinopyroxenes show similar patterns: added aluminum increases some moduli and added iron lowers the diagonal moduli. These trends in amphiboles are further explored through comparison of velocity anisotropy and the hydrostatic-induced strain anisotropy.

6.2 Velocity Anisotropy

Quasi-longitudinal and quasi-transverse wave velocities are shown in Figure 4 as a function of propagation direction in three orthogonal planes. For comparison with current amphibole determinations, velocities for a nearly iron-free chrome-containing diopside based on moduli reported by Isaak *et al.* (2006) are included; the diopside moduli more recently reported by Sang *et al.* (2011) are in close agreement. Velocities based on the elastic moduli of sample I of Aleksandrov and Ryzhova (1961a) are included, as are velocities for glaucophane based on measurements of Bezacier *et al.* (2010). Figure 4

Quasi-longitudinal velocities for both diopside and the amphiboles are uniformly most anisotropic in the X-Z plane (containing the *a*- and *c*-axes) and are most isotropic in the Y-Z plane (containing the *b*- and *c*-axes). Although not fully symmetric, quasi-longitudinal velocities in the X-Z plane are roughly ellipsoidal (although diopside maintains higher velocities over a broader range of directions) with the semi-major axis rotated from alignment with the *c*-axis. The diopside semi-major axis is rotated clockwise (associated with positive values for the uniquely monoclinic moduli C_{15} and C_{35}) while the semi-major axis for all amphiboles is rotated counterclockwise (associated with negative values for C_{15} and C_{35}).

The maximum quasi-longitudinal velocity for both the diopside and the iron-free amphiboles is >9 km/s. All amphiboles are more anisotropic than clinopyroxenes as a result of the small values of moduli associated with the a^* direction (C_{11} C_{12} C_{13} C_{55} and C_{66}). The lowest quasi-longitudinal velocity for tremolite is ~6 km/s in a direction ~20° counter-clockwise from the positive a^*. Pargasite (with more aluminum and full occupancy of the A-site) has a larger minimum velocity of ~7 km/s in roughly the same orientation. Glaucophane quasi-longitudinal velocity anisotropy is intermediate between tremolite and pargasite with the semi-major axis located closer to the *c*-axis. Based on the compositional derivatives in Table 4, velocities for iron-rich amphiboles (ie. ferro-actinolite and ferro-pargasite) are substantially lower (8.4 km/s in the fast direction and 5.3 km/s in the slowest direction) as a result of smaller values for the diagonal moduli and larger densities.

The greater quasi-transverse wave anisotropy for amphiboles than for clinopyroxene is evident in Figure 4. Amphibole quasi-transverse wave anisotropy ranges from a minimum velocity for tremolite of 3.7 km/s and a maximum of 5.2 km/s. Within the *a*-*b* plane quasi-transverse velocities for the two wave polarizations are equal in the a^*-direction and show the greatest difference in the *b*-direction.

As shown in Figure 4, velocities based on the hornblende moduli reported by Aleksandrov and Ryzhova (1961a) do not compare well with the current amphibole data. Quasi-longitudinal velocities are both significantly smaller and have less anisotropy as shown in the *b*-*c* plane. The magnitude of the velocity anisotropy and its orientation relative to crystal axes, as illustrated in the *a*-*c* plane, do not match current data. It is likely that these moduli, like the moduli for the feldspars (as previously discussed in Brown *et al.* 2016 and Waesselman *et al.* 2016) are biased as a result of open cleavage surfaces and cracks.

The moduli for amphiboles reported here and the previously reported moduli for plagioclase (Brown *et al.* 2016) and potassium feldspars (Waeselmann *et al.* 2016), taken together, show that all major crustal mineral phases are highly anisotropic. In fact, they are as anisotropic as the sheet silicates phlogopite (Chheda *et al.* 2014) and muscovite (Vaughan and Guggenheim 1986). Thus, any preferred orientations of minerals will lead to rocks that exhibit significantly anisotropic velocities.

In the absence of data from other sources, all past efforts to understand crustal seismic anisotropy and the anisotropy measured in rocks with preferred crystal orientations have relied on the moduli reported by Aleksandrov and Ryzhova (1961a, 1961b). A pragmatic choice, compensating for the low moduli has been to use the Voigt average (upper elastic aggregate bound) rather than the more appropriate Hill or Hashin-Shtrikman average (see also the discussion in Brown *et al.* 2016 related to plagioclase minerals). As demonstrated in Figure 4, use of the these moduli fails to account for the full anisotropy of the amphiboles in rocks containing crystal preferred orientations. It would appear necessary to recalculate properties of amphibole-rich rocks on the basis of more accurate determinations of amphibole elasticity.

6.3 Isotropic moduli and body wave velocities

Determinations of bulk moduli for several calcium and sodium amphibole compositions are summarized in Table 7. For these highly anisotropic minerals, the Reuss-bound bulk moduli, measured in isothermal compression experiments, are significantly smaller that the adiabatic Hashin-Shtrikman (or Hill average of Voigt and Reuss bounds) moduli appropriate for calculation of elastic wave speeds. Current Reuss-bound adiabatic bulk moduli are corrected to isothermal conditions using thermodynamic properties summarized in Hacker *et al.* (2003b) (a reduction of about 1.5%). The mean adiabatic Hashin-Shtrikman (H-S) moduli are nearly 10% greater. The moduli determined under isothermal compression by Comodi *et al.* (1991) appear to better match the current H-S estimates. However, a reanalysis of these data for glaucophane gave a modulus more in accord with the Reuss-bound value based on elastic moduli. Jenkins *et al.* (2010) also measured lattice strains in two synthetic glaucophane crystals to 10 GPa and reported an isothermal bulk modulus that is only slightly larger than the Reuss-bound estimate.

Table 7

In Table 8 current values of the adiabatic shear modulus for several calcium and sodium amphibole compositions are compared with Hacker *et al*. (2003b). Their compilation, based on an assumed value of Poisson's ratio, consistently under-estimates the shear modulus for all amphiboles; this would lead to an under-prediction of transverse wave velocities.

Table 8

Isotropic body wave velocities, compressional (V_p) and shear (V_s), for the calcium and sodium amphiboles, listed in Table 9, exhibit clear trends. Increasing aluminum content leads to higher compressional velocities while aluminum content has less impact on shear wave velocities. Increasing iron content decreases both compressional and shear wave velocities. The prior estimates are not consistent with these trends. That the estimate for hornblende, as an average calcium amphibole, has lower density and higher sound speeds than the hornblendite of Christensen (1996) might reflect a compositional difference. With more aluminum and more iron, the prediction can be moved in the appropriate direction to better match the hornblendite velocities. Table 9

Poisson's ratio, $\sigma = \frac{1}{2}\left[1 - \left(\left(\frac{V_p}{V_s}\right)^2 - 1\right)^{-1}\right]$, was identified by Christensen (1996) as an important discriminator in the interpretation of crustal seismology. The near constant value assumed by Hacker *et al.* (2003), when no independent determination of the shear modulus was available, is not supported in the current work. Poisson's ratio ranges from 0.20 to 0.27. It decreases strongly with iron content and increases modestly with aluminum content. The sodium amphibole, glaucophane, has the smallest value.

The comparisons made in this section suggest that the predicted isotropic body wave velocities of an average calcium amphibole (hornblende) based on the compositional dependences determined here are in reasonable agreement with laboratory measurements on a hornblendite of unspecified composition. Prior efforts were not able to correctly describe the variation of isotropic elastic wave velocities within the range of amphibole compositions found in crustal rocks.

6.4 Anisotropic strain under hydrostatic stress

Projections on two planes of elastic compressibilities under hydrostatic stress are shown in Figure 5 using the compliance sums, β_i, of Table S2. Three amphiboles (tremolite, pargasite, and glaucophane) and one clinopyroxene (diopside) are plotted. All amphiboles have the most compliant direction aligned between a^*- and c-axes. The semi-major axis of glaucophane is rotated least from a^* and tremolite is rotated most. Although the synthetic glaucophane axes compression measurements show near isotropic strain in the b-c plane, the elastic moduli predict significant anisotropy that is similar to pargasite. Tremolite in the b-c plane has intermediate anisotropy. The weaker bonding of amphiboles (with vacant or partially filled A- sites) allows greater strains in the general a-axis direction. The structurally and compositionally similar mineral diopside is less compliant in this direction. In the a-c plane, the most and least compressible directions for diopside are rotated by nearly 90° relative to the amphiboles. Figure 5

The comparisons made in this section indicate that compressibilities under hydrostatic compression calculated on the basis of elastic moduli measured at ambient pressure are in general accord with x-ray measurements made at high pressure. However, axes compliances (and the resulting bulk moduli) based on x-ray compression measurements are sensitive to the form of equations of state used to fit the data (*e.g.* multiple entries in Table 7 and in Jenkins *et al.* 2010). Such

uncertainty can explain the error in the compositional behavior that was previously associated with amphiboles in the compilation by Hacker *et al.* (2003b) when these measurements provided the only information related to elastic properties of important amphibole end member phases.

7. Summary

The full single-crystal elastic moduli of nine natural calcium to calcium-sodium amphiboles have been measured. In addition, velocities of a previously studied natural sodium amphibole have been re-analyzed within the computational framework used in the current study. Clear trends in the behavior of moduli of the calcium and calcium-sodium amphiboles as a function of composition have been identified. A linear fit based on three chemical measures (total aluminum, total iron, and A-site occupation) accounts for most of the compositionally-induced variance in moduli. Separating contributions of aluminum in C- and T-sites is not significant at the 95% confidence level. A linear fit in composition could not reconcile the sodium amphibole glaucophane with the other calcium-sodium amphiboles.

The amphiboles and chemically related clinopyroxenes share similar values of moduli except that amphibole moduli related to the a^* direction (C_{11}, C_{12}, C_{13}, C_{55}, *and* C_{66}) are approximately a factor of two smaller. This is likely associated with the partially occupied or vacant A-site which is associated with bonding in the *a*-axis direction. Increasing occupation of the A-site increases some of these moduli. In contrast, the substitution of sodium for calcium in the B-site has no significant impact on moduli. The substitution of iron in the C-sites decreases all diagonal elastic moduli while leaving off-diagonal moduli unaffected.

The orientation of quasi-longitudinal velocity extrema in the *a*-*c* plane is significantly rotated between the amphiboles and the clinopyroxenes. This difference is associated with a large negative value of C_{35} for amphiboles and a large positive value for clinopyroxenes.

Since the variation of isotropic elastic behavior of amphiboles with composition is important in interpretations of crustal seismology, parameters are provided that allow accurate determination of the isotropic bulk and shear moduli of common amphiboles in crustal rocks.

It is noteworthy that amphiboles have higher elastic wave velocities and are more anisotropic than suggested by the early ultrasonic measurements. In fact, amphiboles exhibit anisotropy nearly as large as that observed in sheet silicates and the feldspars. In efforts to reconcile laboratory measurements on rocks with predictions based on the single-crystal moduli reported by Aleksandrov and Ryzhova (1961a and 1961b), the *ad-hoc* use of the upper-bound Voigt average is common. This provided partial, but inappropriate, compensation for moduli subject to systematic experimental bias. Furthermore, analyses based on the earlier moduli failed to account for the full anisotropy of amphiboles. Thus, all predictions of the seismic response of rocks with preferred crystal orientations will need to be re-evaluated.

Acknowledgments

Support from the National Science Foundation EAR-0711591 enabled this research. The following students helped prepare samples and collect data: N. Castle, E. Chang, S. Pendleton, K. Pitt, K. Straughan, A. Teel, and H. West-Foyle. The microprobe analyses of S. Kuehner and N. Castle and x-ray analyses of W. Kaminsky were vital contributions to this work. B.W. Evans contributed samples and maintained continuing discussions. The RRUFF database and materials provided by R. Downs are highly appreciated. This research was inspired by a course offered by N. I. Christensen in 1974 on the elasticity of minerals and seismic structure of the crust. It was co-attended by M. Salisbury, D. Fountain, and R. L. Carlson. The science contributions and continued enthusiasm of these colleagues is gratefully acknowledged.

References

Abramson, E. H., Brown, J. M., and Slutsky, L. J. (1999) Applications of impulsive stimulated scattering in the Earth and planetary sciences, Annu. Rev. Phys. Chem., 50, 279–313.

Aleksandrov, K. S., Ryzhova, T. V. (1961a) The elastic properties of rock-forming minerals: pyroxenes and amphiboles, Bulletin. USSR Academy of Science, Geophysics, Ser. 9, 871–875.

Aleksandrov, K. S., Ryzhova, T. V. (1961b) Elastic properties of rock-forming minerals II. Layered silicates, Bulletin. USSR Academy of Science, Geophysics, Ser. 9, 1165-1168.

Angel R. J. (2001) EOS-FIT V5.2 users guide. http://www.crystal.vt.edu/crystal/software.html. Program revision August 2008

Audet P., Bostock M. G., Boyarko D. C., Brudzinski M. R. and Allen R. M. (2010) Slab morphology in the Cascadia fore arc and its relation to episodic tremor and slip. J. Geophys. Res., **115**,

Barberini, V., Burlini, L., Zappone, A. (2007) Elastic properties, fabric and seismic anisotropy of amphibolites and their contribution to the lower crust reflectivity, Tectonophysics, 445, 227–244.

Bezacier, L., Reynard, B., Bass, J. D., Wang, J., Mainprice, D. (2010) Elasticity of glaucophane, seismic velocities and anisotropy of the subducted oceanic crust, Tectonophysics, 494, 201–210.

Brown, J.M., Slutsky, L. J., Nelson, K.A.,and Cheng, L-T. (1989) Single crystal elastic constants for San Carlos Peridot: An application of impulsive stimulated scattering, J. Geophys. Res., 94, 9485-9492.

Brown, J. M. (2015), Determination of Hashin-Shtrikman bounds on the isotropic effective elastic moduli of polycrystals of any symmetry, Comput. Geosci., 80, 95–99, doi:10.1016/j.cageo.2015.03.009.

Brown, J.M., (2016) Determination of elastic moduli from measured acoustic velocities, Comput. Geosci., submitted

Brown, J. M., Angel, R. J., and Ross, N. L. (2016) Elasticity of plagioclase feldspars, J. Geophys. Res. Solid Earth, 121, doi:10.1002/2015JB012736.

Brown, J. M., Abramson, E. H., Ross, R. L. (2006) Triclinic elastic constants for low albite, Phys. Chem. Minerals, 33, 256-265.

Chheda, T. D., Mookherjee, M., Mainprice, D., dos Santos, A. M., Molaison, J. J., Chantel, J., Manthilake, G., Bassett, W. A. (2014), Structure and elasticity of phlogopite under compression: Geophysical implications, Phys. Earth Planet. Int., 233, 1-12, doi:10.1016/j.pepi.2014.05.004

577 Christensen, N. I., and Mooney, W. D. (1995) Seismic velocity structure and
578 composition of the continental crust: A global view, J. Geophys. Res., 100, 9761–
579 9788.

580 Christensen, N. I. (1996) Poisson's ratio and crustal seismology, J Geophys. Res., 101,
581 3139-3156.

582 Collins, M. C., and Brown, J. M. (1998) Elasticity of an upper mantle clinopyroxene,
583 Phys. Chem. Min., 26, 7-13.

584 Comodi, P., Mellini, M., Ungaretti, L., Zanazzi, P.F. (1991) Compressibility and high
585 pressure structure refinement of tremolite, pargasite and glaucophane, Eur. J.
586 Mineral., 3, 485–499.

587 Hacker, B. R., Peacock, S. M., Abers, G. A. and Holloway, S. D. (2003a) Subduction
588 factory, 2, Are intermediate-depth earthquakes in subducting slabs linked to
589 metamorphic dehydration reactions?, J. Geophys. Res., 108, 2030,
590 doi:10.1029/2001JB001129.

591 Hacker, B. R., Abers, G. A. & Peacock, S. M. (2003b). Subduction factory, 1,
592 Theoretical mineralogy, density, seismic wave speeds, and H_2O content. J. Geophys.
593 Res., 108, 2029, doi:10.1029/2001JB001127.

594 Hawthorn, F.C., Oberti, R. (2007) Amphiboles: Crystal chemistry, Rev. Mineral. &
595 Geochem., 67, 1-54.

596 Hawthorne, F.C., Oberti, R., Harlow, G.E., Maresch, W. V., Martin, R. F., Schumacher, J.
597 C., Welch, M. D. (2012) Nomenclature of the amphibole supergroup, Am. Mineral.,
598 97, 2031–2048.

599 Holland, T. J. B., and Powell, R. (1998) An internally consistent thermodynamic data
600 set for phases of petrological interest, J. Metamorph. Geol., 16, 309–343, 1998.

601 Isaak, D. G., Ohno, I., Lee, P.C. (2006) The elastic constants of monoclinic single-
602 crystal chrome-diopside to 1,300 K, Phys. Chem. Miner., 32, 691–699 DOI
603 10.1007/s00269-005-0047-9.

604 Jenkins, D. M., Corona, J. C., Bassett, W. A., Mibe, K., Wang, Z. (2010) Compressibility
605 of synthetic glaucophane, Phys. Chem. Minerals, 37, 219–226 DOI 10.1007/s00269-
606 009-0326-y.

607 Ji, S., Shao, T., Michibayashi, K., Long, C., Wang, Q., Kondo, Y., Zhao, W., Wang, H., and
608 Salisbury, M.H. (2013) A new calibration of seismic velocities, anisotropy, fabrics,
609 and elastic moduli of amphibole-rich rocks, J. Geophys. Res.: Solid Earth, 118, 4699–
610 4728, doi:10.1002/jgrb.50352, 2013

611 Kandelin, J., Weidner, D. J. (1988a) Elastic properties of hedenbergite, J. Geophys.
612 Res., 93, 1063-1072.

613 Kandelin, J., Weidner, D. J. (1988b) The single crystal properties of jadeite, Phys.
614 Earth Planet. Inter., 50, 251-260.

615 Leake, B.E., Woolley, A.R., Arps, C. E. S. Birch, W. D., Gilbert, M. C., Grice, J. D.,
616 Hawthorne, F. C. Kato, A., Kisch, H. J. Krivovichev, V. G. Linthout, K., Laird, J.
617 Mandarino, J. A., Maresch, W. V., Nickel, E. H., Rock, N. M. S., Schumacher, J. C., Smith,
618 D. C., Stephenson, N. C. N., Ungaretti, L., Whittaker, E. J. W., Youzhi, G., (1997)
619 Nomenclature of amphiboles: Report of the subcommittee on amphiboles of the
620 International Mineralogical Association Commission on New Minerals and Mineral
621 Names, Canadian Mineral., 35, 219-246.

622 Llana-Funez, S., Brown, D. (2012) Contribution of crystallographic preferred
623 orientation to seismic anisotropy across a surface analog of the continental Moho at
624 Cabo Ortegal, Spain, Geol. Soc. Amer. Bul., 124, 1495-1513

625 Rencher, A. C. (2002) Methods of Multivariable Analysis, John Wiley & Sons, New
626 York.

627 Sang, L., Vanpeteghem, C.B., Sinogeikin, S.V., and Bass, J.D. (2011) The elastic
628 properties of diopside, $CaMgSi_2O_6$, Am. Mineral., 96*, 224–227*

629 Schumacher, J.C. (2007) Metamorphic amphiboles: Composition and coexistence,
630 Rev. Min. & Geochem, 67, 359-416.

631 Selway, K., Ford, H., Kelemen, P. (2015) The seismic mid-lithosphere discontinuity,
632 Earth Planet. Sci. Lett., 414, 45-57.

633 Seront, B., Mainprice, D., and Christensen, N. I. (1993), A determination of the 3-
634 dimensional seismic properties of anorthosite—Comparison between values
635 calculated from the petrofabric and direct laboratory measurements, J. Geophys.
636 Res., 98, 2209–2221, doi:10.1029/92JB01743.

637 Tatham, D. J., Lloyd, G. E., Butler, R. W. H., Casey, M. (2008) Amphibole and lower
638 crustal seismic properties, Earth Planet. Sci. Lett., 267, 118–128

639 Tindle, A.G., Webb, P.C. (1994) Probe-AMPH—A spreadsheet program to classify
640 microprobe-derived amphibole analyses, Comput. & Geosci., 20, 1201-1228.

641 Vaughan, M.T., Guggenheim, S. (1986) Elasticity of muscovite and its relationship to
642 crystal structure. J. Geophys. Res. 91, 4657–4664.

643 Waeselmann, N, Brown, J. M., Angel, R, J., Ross, N., Zhao, J., and Kaminsky, W. (2016)
644 The elastic tensor of monoclinic alkali feldspars, Am. Mineral., doi:10.2138/am-
645 2015-5583.

646 Watt, J. P., Davies, G. F. and O'Connell, R. J. (1976) The elastic properties of
647 composite materials, Rev. Geophys. Space Phys., 14, 541-563.

648 Watt, J. P. and O'Connell, R. J. (1980) An experimental investigation of the Hashin-
649 Shtrikman bounds on two-phase aggregate elastic properties, Phys Earth Planet Int.,
650 21, 359-370.

Figures

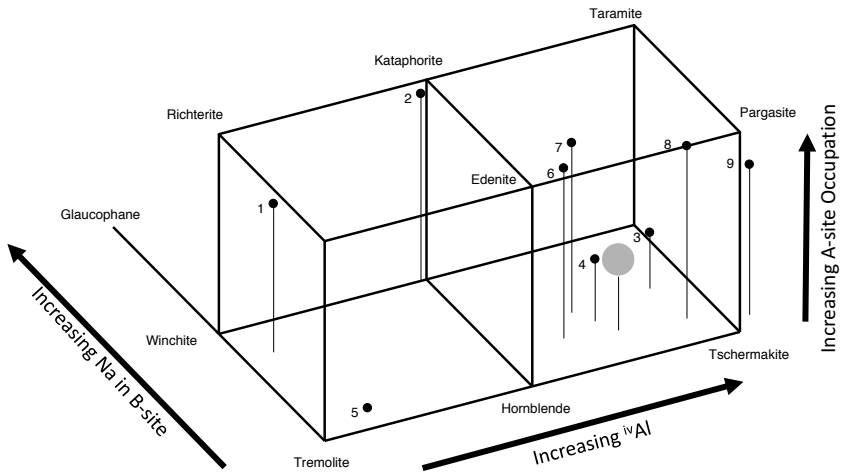

Figure 1. Classification and compositions of magnesium calcium amphiboles plus glaucophane (based on Leake et al. 1997). The axis extending to the right gives increasing aluminum in tetrahedral coordination (from 0 for tremolite to ($Al_2Si_6O_{22}$) for tschermakite). Occupancy of the A-site by (Na+K) (from 0 to 1) is shown in the vertical direction. Substitution of Na for Ca in the B-site extends into the figure with full replacement of Ca by Na found in glaucophane. Named stoichiometric end-member compositions are identified. Full solid-solution replacement of magnesium by iron is labeled by adding ferro- to the end-member names (exceptions ferro-actinolite is the iron-bearing form of tremolite). Small filled and numbered circles are compositions of the current samples based on the chemistry provided in Table 2. The large gray circle gives the average chemistry for calcium amphiboles reported by Schumacher (2007). Lines projected to the zero of A-site occupation are provided as an aid in visualizing the sample compositions.

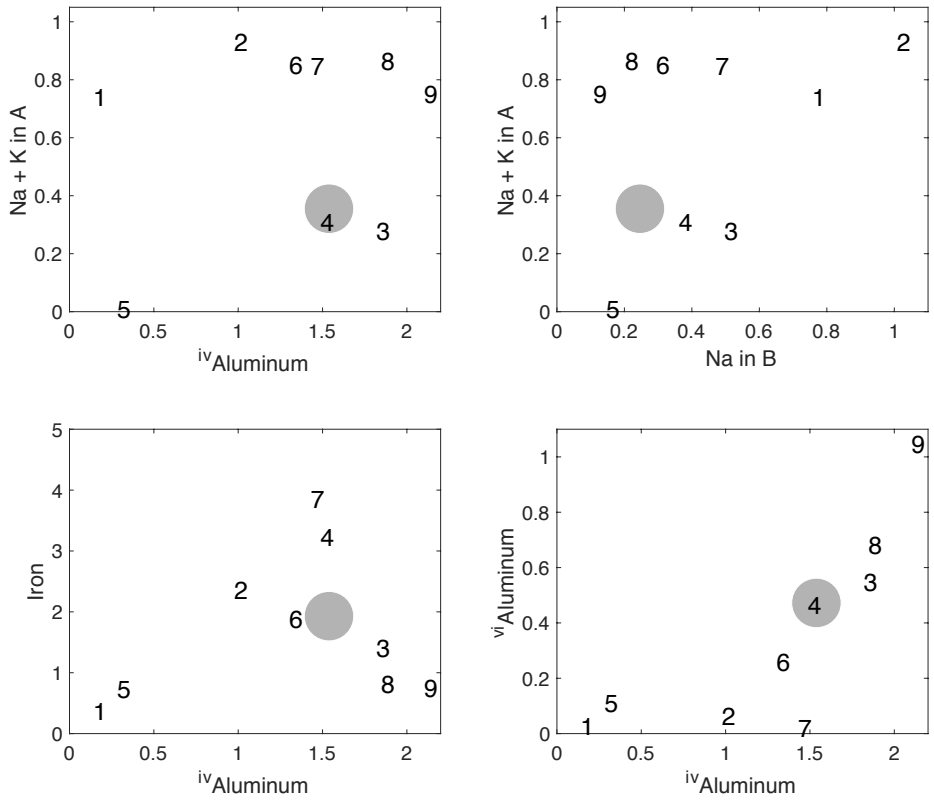

Figure 2. Compositions of the amphibole samples in formula units reported in Table 2. Plotted numbers correspond to the sample numbers. The gray circle is the average of calcium amphiboles reported by Schumacher (2007). The top two panels show front and side projections of the compositions illustrated in Figure 1 (tetrahedral coordinated aluminum versus A-site occupation and sodium in the B-site vs A-site occupation). The lower left panel shows the number of iron atoms per formula unit vs tetrahedral coordinated aluminum. The lower panel on the right shows octahedral-coordinated aluminum versus tetrahedral-coordinated aluminum.

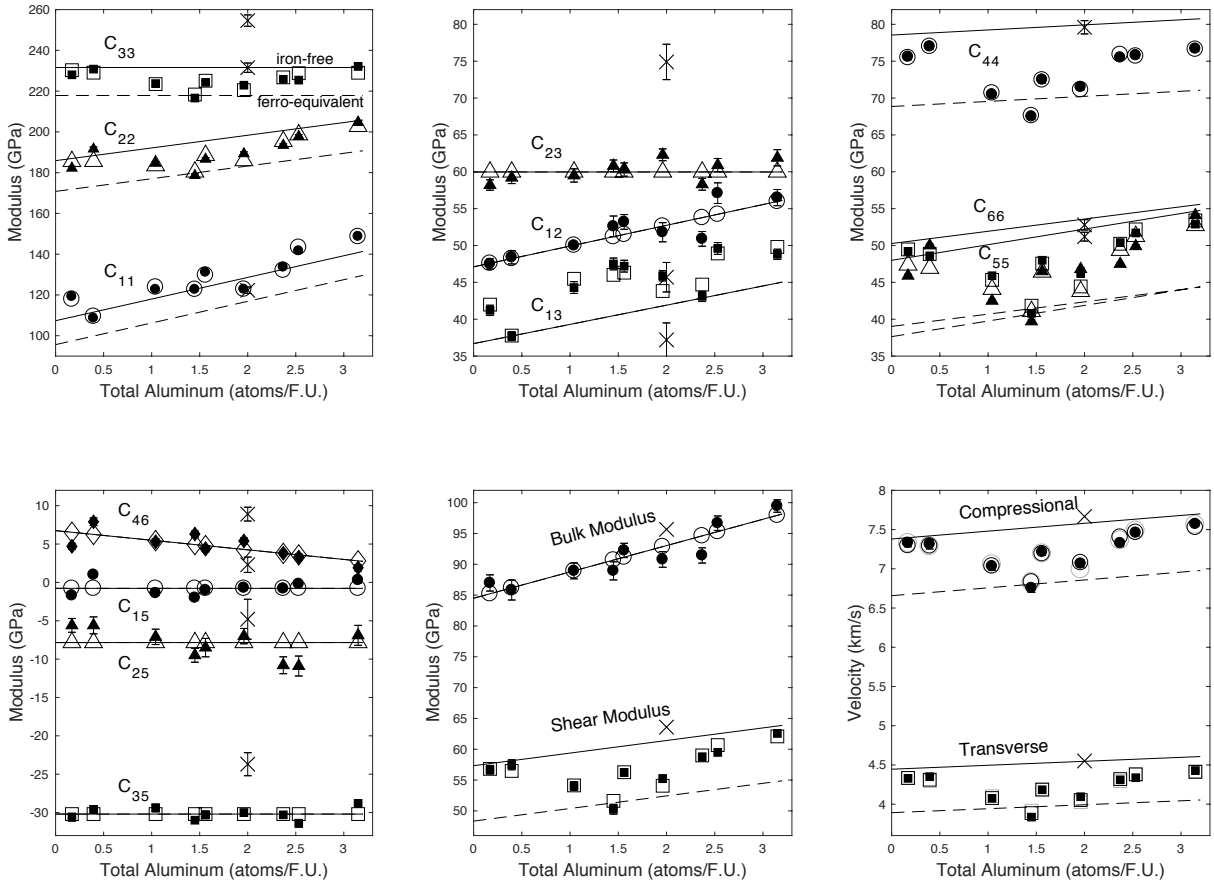

675

676 Figure 3. Elastic moduli and velocities of amphiboles as a function of total aluminum.
677 Filled symbols are current experimental results with 2σ uncertainties shown when
678 larger than the plotted symbol. Different symbols are associated with particular
679 moduli as labeled in each panel. Points with the X symbols are moduli and velocities
680 for glaucophane (Bezacier *et al.* 2010). Open symbols give the predictions. As
681 indicated only in the upper left panel, solid lines are predictions for increasing
682 aluminum content in an iron-free mineral with no A-site occupation. Dashed lines
683 (when present) give the predicted ferro-equivalent behavior.

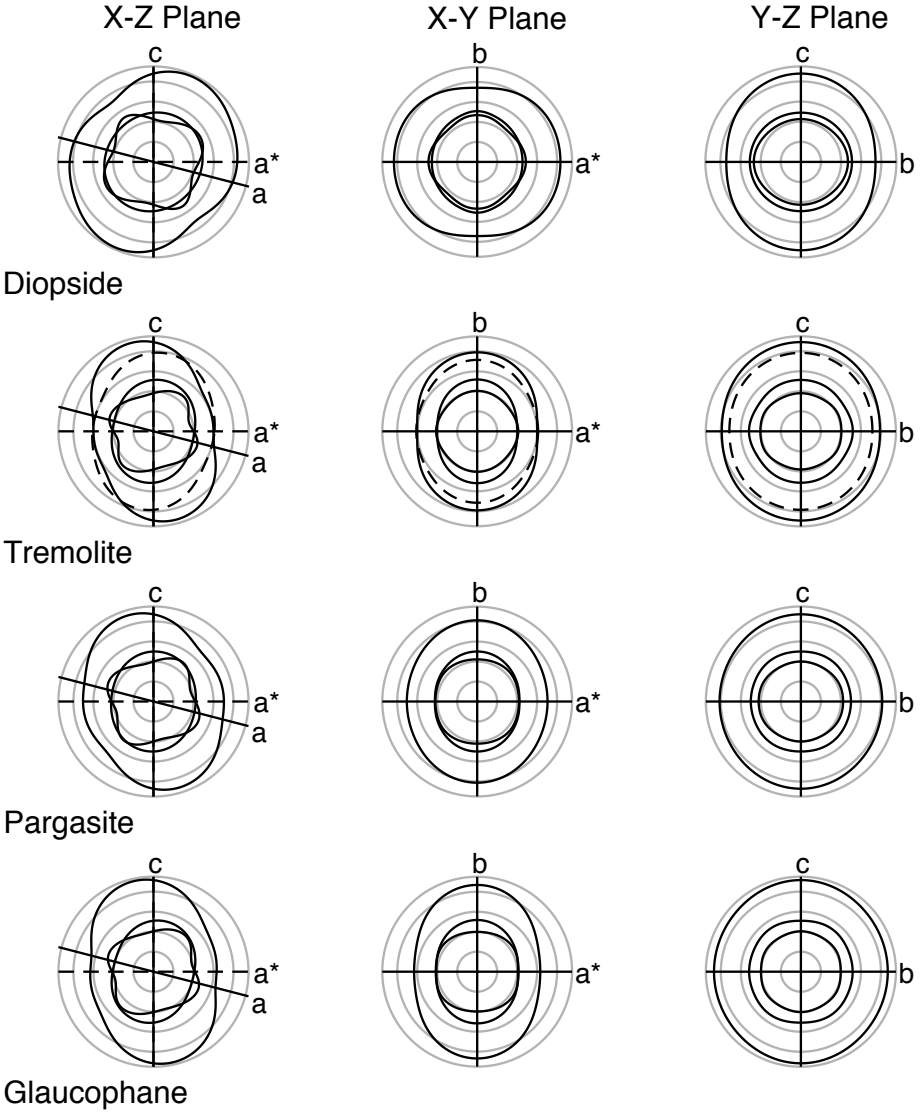

684

685 Figure 4. Selected inosilicate elastic wave velocities as a function of propagation
686 direction in three orthogonal planes. For each plane normal to a Cartesian axis light
687 circles represent velocities of 2, 4, 6, 8, and 9.5 km/s. The orientations of
688 crystallographic axes are shown. Thick lines are velocities based on the elastic
689 moduli and propagation directions. The inner thick lines are quasi-transverse wave
690 velocities, the outer thick line gives quasi-longitudinal velocities. Top row: diopside
691 velocities based on Isaak *et al.* (2006). Second and third rows: calcium amphibole
692 end-member velocities based on the current work. Dashed lines in second row are
693 quasi-longitudinal velocity predictions based on the elastic moduli for a hornblende
694 reported by Aleksandrov and Ryzhova (1961a). Bottom row: glaucophane velocities
695 based on Bezacier *et al.* (2010).

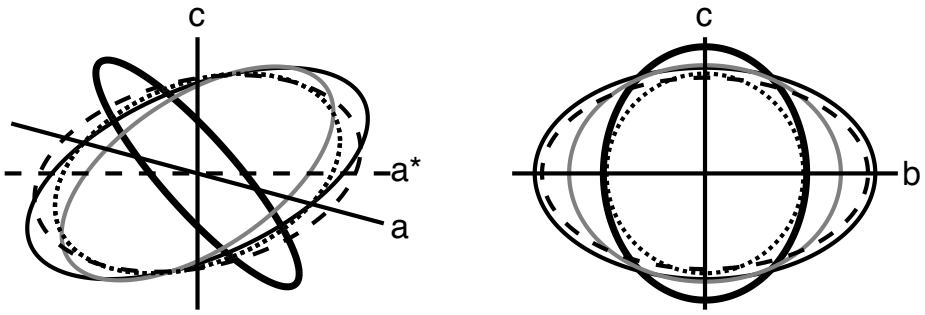

Figure 5. Selected inosilicate strain ellipsoids under hydrostatic stress projected on the crystallographic *a*-*c* and *b*-*c* planes. Thick solid line: diopside from Isaak *et al.* (2006), solid line: tremolite from current work, grey line: pargasite from current work), dashed line: glaucophane based on Bezacier *et al.* (2010), dotted line: glaucophane based on Jenkins *et al.* (2010).

Tables

Sample	Unit cell volume (A°^{3})	a (A°)	b (A°)	c (A°)	β (°)	Density kg/m^3	Source
1	905.7	9.88	17.98	5.27	104.6	3027	unknown
2	914.3	9.87	18.03	5.31	104.6	3255	unknown
3	901.9	9.80	17.98	5.29	104.9	3162	Gore Mountain NY, collected by B.W. Evans
4	913.6	9.83	18.08	5.32	104.9	3293	unknown
5	908.4	9.84	18.02	5.29	104.6	3038	Lake Wenatchee, WA collected by B.W. Evans
6	918.1	9.91	18.08	5.31	105.1	3213	RRuff.info #60029 R. Downs
7	934.0	9.96	18.21	5.33	104.9	3418	RRuff.info #60044 R. Downs
8	907.2	9.86	17.99	5.30	105.3	3163	RRuff.info #60632 R. Downs
9	895.2	9.80	17.92	5.28	105.2	3190	Unknown

Table 1. Amphibole sample information. Samples of "unknown" source were obtained as mineral separates from rocks of unknown origin. Unit cell volumes and cell parameters are from x ray analysis, densities are calculated based on unit cell volumes and the microprobe determination of chemistry. Individual crystals from the same source exhibited variations in cell parameters of about 0.01 A°. Based on this variability an uncertainty in the unit cell volume is 0.3%. The density uncertainty, accounting for chemistry and volume uncertainties, is 0.5%.

Sample	1	2	3	4	5	6	7	8	9	GL	HBL
Structural Formulae											
Si	7.859	7.023	6.182	6.513	7.718	6.698	6.571	6.152	5.898	7.76	6.458
Al^{iv}	0.141	0.977	1.818	1.487	0.282	1.302	1.429	1.848	2.102	0.24	1.542
Al^{vi}	0.032	0.064	0.553	0.464	0.113	0.259	0.015	0.683	1.047	1.76	0.470
Ti	0.013	0.109	0.112	0.173	0.002	0.060	0.239	0.319	0.021	-	0.123
Cr	0.000	0.002	0.001	0.000	0.035	0.000	0.000	0.002	0.211	-	0.001
Fe^{3+}	0.097	0.769	1.263	0.727	0.494	0.365	0.559	0.000	0.157	-	0.718
Fe^{2+}	0.287	1.601	0.150	2.004	0.244	1.526	3.298	0.815	0.592	0.92	1.201
Mn	0.028	0.157	0.012	0.030	0.040	0.049	0.205	0.007	0.013	-	0.034
Mg	4.543	2.298	2.910	1.601	4.072	2.741	0.684	3.105	2.958	2.34	2.453
Ca	1.243	0.993	1.503	1.639	1.741	1.706	1.528	1.798	1.892	0.06	1.752
Na	1.236	1.674	0.683	0.577	0.146	0.805	0.981	0.696	0.789	1.90	0.480
K	0.264	0.265	0.088	0.095	0.009	0.341	0.339	0.370	0.071	-	0.121
F	0.937	0.695	0.000	0.000	0.035	0.732	0.000	0.263	0.005	-	0.000
Cl	0.002	0.015	0.000	0.008	0.000	0.030	0.000	0.005	0.000	-	0.000
OH*	1.060	1.290	2.000	1.992	1.965	1.238	2.000	1.732	1.995	2	2.000
Total	17.743	17.932	17.275	17.310	16.895	17.852	17.848	17.795	17.752	-	17.353
Site Occupancy											
(Ca+Na) (B)	2.000	2.000	2.000	2.000	1.887	2.000	2.000	2.000	2.000	1.96	2.000
Na (B)	0.757	1.007	0.497	0.361	0.146	0.294	0.472	0.202	0.108	1.90	0.248
(Na+K) (A)	0.743	0.932	0.275	0.310	0.009	0.852	0.848	0.864	0.752	-	0.353
$Mg/(Mg+Fe^2)$	0.941	0.589	0.951	0.444	0.943	0.642	0.172	0.792	0.833	-	0.671
$Fe^3/(Fe^3+Al^{vi})$	0.750	0.923	0.696	0.610	0.814	0.585	0.974	0.000	0.130	-	0.604

Table 2. Microprobe chemical analysis of nine calcium and calcium-sodium amphiboles in formula units (basis of 22 oxygens) using Probe-AMPH (Tindle and Webb, 1994) plus the chemical analysis of glaucophane (GL) reported in Bezacier *et al.* (2010) and the average calcium amphibole (HBL) as reported by Schumacher (2007). See supplemental table for weight % oxides measured by microprobe analysis.

	1	2σ	2	2σ	3	2σ	4	2σ	5	2σ	6	2σ	7	2σ	8	2σ	9	2σ	Gl	2σ
C_{11}	119.2	0.8	122.7	0.9	133.6	0.9	122.8	0.9	108.6	0.7	131.1	0.9	122.7	0.9	141.6	0.9	148.7	1.0	121.5	1.6
C_{12}	47.5	0.7	50.0	0.3	50.9	1.0	51.8	1.3	48.4	0.9	53.2	1.0	52.6	1.4	57.1	1.4	56.5	1.1	44.4	2.0
C_{13}	41.2	0.7	44.3	0.8	43.1	0.7	45.9	0.7	37.7	0.6	47.2	0.8	47.5	0.8	49.6	0.8	48.8	0.7	37.4	2.3
C_{15}	-1.7	0.3	-1.4	0.3	-0.8	0.3	-0.7	0.3	1.0	0.3	-1.0	0.3	-2.0	0.3	-0.2	0.3	0.3	0.4	2.7	1.0
C_{22}	182.2	1.3	184.6	1.2	193.4	1.2	189.3	1.3	191.6	1.4	186.6	1.2	178.6	1.2	197.8	1.3	204.6	1.3	229.7	2.3
C_{23}	58.2	0.8	59.5	0.9	58.3	0.9	62.3	0.9	59.2	0.9	60.3	0.9	60.8	0.9	60.9	1.0	61.9	1.1	75.8	2.4
C_{25}	-5.6	0.9	-7.1	1	-10.8	1.1	-7.0	1.0	-5.6	1.1	-8.5	1.2	-9.5	0.9	-10.9	1.3	-6.9	1.3	-4.9	2.6
C_{33}	228.0	1.5	223.7	1.5	225.8	1.4	222.9	1.4	230.8	1.5	224.3	1.4	216.6	1.3	225.4	1.6	232.1	1.5	256.2	2.8
C_{35}	-30.6	0.5	-29.4	0.5	-30.3	0.4	-30.0	0.4	-29.6	0.5	-30.3	0.5	-31.0	0.4	-31.4	0.5	-28.8	0.5	-23.9	1.5
C_{44}	75.6	0.6	70.5	0.5	75.5	0.6	71.5	0.5	77.0	0.6	72.5	0.6	67.5	0.5	75.8	0.6	76.7	0.6	79.3	0.9
C_{46}	4.7	0.4	5.3	0.4	3.8	0.3	5.4	0.4	7.9	0.5	4.4	0.4	6.3	0.4	3.3	0.4	1.9	0.4	9.3	0.9
C_{55}	45.9	0.3	42.5	0.3	47.5	0.3	46.8	0.3	50.0	0.3	46.5	0.3	39.7	0.3	49.9	0.3	54.1	0.3	52.9	0.7
C_{66}	49.2	0.4	45.9	0.3	50.4	0.3	46.2	0.4	48.6	0.4	48.0	0.4	40.8	0.3	51.7	0.4	52.9	0.4	51.3	0.6

Table 3. Elastic moduli (in GPa) of amphiboles. The 2σ uncertainties include misfits to velocities and uncertainty in sample densities. The column labeled "Gl" gives re-analyzed moduli and uncertainties for glaucophane based on velocities reported by Bezacier et al (2010).

	Modulus GPa	*dM/dAl* GPa/atom	*dM/dA* GPa/atom	*dM/dFe* GPa/atom	Experimental Uncertainty GPa	Regression Misfit GPa
C_{11}	107.2	10.6	13.3	-2.9	1.0	1.1
	109.1	11.4			1.0	5.0
C_{12}	47.1	2.8			1.2	1.6
C_{13}	36.7	2.6	6.5		0.8	1.2
	39.6	3.1			0.8	2.4
C_{15}	-0.8				0.3	0.9
C_{22}	185.9	6.2		-3.8	1.2	2.7
C_{23}	60.0				1.0	1.4
C_{25}	-7.8				1.2	1.9
C_{33}	231.6			-3.4	1.5	2.1
C_{35}	-30.2				0.5	0.8
C_{44}	78.5	0.7	-3.0	-2.4	0.6	0.2
	78.0			-2.5	0.6	1.1
C_{46}	6.7	-1.3			0.4	1.1
C_{55}	48.0	2.1		-2.6	0.4	1.9
C_{66}	50.3	1.7		-2.8	0.4	0.8
K	84.5	4.3			1.2	1.7
G	57.5	2.0		-2.2	0.8	0.8

720

721 Table 4. Linear regression parameters for amphibole individual elastic moduli and
722 the mean of Hashin-Shtrikman bounds for the adiabatic bulk (K) and shear (G)
723 modulus. Base moduli for tremolite are in the first column of values. Derivatives are
724 in units of modulus change per substitutional atom in the formula unit relative to
725 tremolite; the aluminum content varies from 0 to >3, the A-site occupation ranges
726 from 0 to 1, and iron in the C-site can range from 0 to 5. Only C_{11}, C_{13} , and C_{44} have a
727 statistically significant dependence on the A-site occupation. An alternative fit with
728 no dependence on A-site occupation is provided (with a concomitant increase in
729 misfit). The last two columns give experimental and regression misfits.

730

	M	*dM/dAl*	*dM/dA*	*dM/dFe*	Experimental Uncertainty	Regression Misfit
Density (kg/m^3)	2974	42	6	58	15	7
	2928	76		158	15	157
V_p (m/s)	7380	100		-181	47	40
V_s (m/s)	4446	50	-113	-138	24	26
	4379	46		-137	24	44

731

732 Table 5. Linear regression parameters for densities, and compressional and
733 transverse wave velocities of the amphiboles. Derivatives are in units of change per
734 substitutional atom in the formula unit relative to tremolite; the aluminum content
735 varies from 0 to >3, the A-site occupation ranges from 0 to 1, and iron in the C-site
736 can range from 0 to 5. Density and transverse wave velocities have a statistically
737 significant dependence on the A-site occupation. An alternative fit with no
738 dependence on A-site occupation is provided (with a concomitant increase in misfit).
739 The last two columns give experimental and regression misfits.

740

	C_{11}	C_{12}	C_{13}	C_{15}	C_{22}	C_{23}	C_{25}	C_{33}	C_{35}	C_{44}	C_{46}	C_{55}	C_{66}
Diopside Isaak *et al.* 2006	228	79	70	8	181	61	6	245	40	79	6	68	78
Tremolite	107	47	37	-1	186	60	-8	232	-30	79	7	48	50
Hedenbergite Kandelin and Weidner 1988a	222	69	79	12	176	86	13	249	26	55	-10	63	60
Actinolite	93	47	37	-1	167	60	-8	215	-30	67	7	35	36
Jadeite Kandelin and Weidner 1988b	274	94	71	4	253	82	14	282	28	88	13	65	94
Glaucophane Bezacier *et al.* 2010	122	46	37	2	232	75	-5	255	-24	80	9	53	51
$Di_{72}Hd_9Jd_3Cr_3Ts_{12}$ Collins and Brown 1998	238	84	80	9	184	60	10	230	48	77	8	73	82
$Tr_{72}Ac_9Pg_{19}$	122	48	44	-1	185	60	-8	228	-30	74	6	46	48

741

742 Table 6. Comparison of amphibole and clinopyroxene elastic moduli in GPa units.
743 Amphibole moduli are calculated using parameters given in Table 4.

	tremolite	ferro-actinolite	hornblende	tschermakite	pargasite	glaucophane	ferro-glaucophane
Current: Reuss	78(1)	78(1)	88(1)	88(1)	94(1)	88(1)	
H-S	85(1)	85(1)	93(1)	93(1)	99(1)	96(1)	
C91	85				97	96 88(6)	
J10						92(2)	
H03	85	76	94	76	91	96	89

744

745 Table 7. Bulk moduli (GPa units) for selected amphiboles. "Current: Reuss" are
746 isothermal values using the parameters in Table 4 and from Bezacier *et al.* (2010).
747 An adiabatic to isothermal correction was applied to the adiabatic moduli using the
748 thermodynamic properties summarized in Hacker *et al.* (2003b). H-S are the
749 average of adiabatic Hashin-Shtrikman bounds. In the current work "hornblende" is
750 a composition based on the Schumacher (2007) average calcium amphibole. The
751 Comodi *et al.* (1991) (C91) and Jenkins *et al.* 2010 (J10) values are based on high
752 pressure isothermal x ray compression measurements. Comodi *et al.* reported
753 values based on linear fits to the data. The second estimate in the C91 row is the re-
754 analysis given by Jenkins *et al.* using a second-order finite-strain equation of state
755 using EoSFit5.2 (Angel 2001). In the last row (H03) isothermal moduli are taken
756 from Table 1 of Hacker *et al.* (2003b). Uncertainties for the current work are from
757 Table S2. The uncertainties for moduli based on axes compression measurements
758 are reported by Jenkins *et al.* (2010).

759

	tremolite	ferro-actinolite	hornblende	tschermakite	pargasite	glaucophane	ferro-glaucophane
Current	58	47	57	62	64	64	
H03	49	44	55	44	53	56	52

760

761 Table 8. Adiabatic shear moduli (GPa units) for selected amphibole end-members. In
762 the current work "Hornblende" designates a mineral composition based on the
763 Schumacher (2007) average calcium amphibole. The top row lists means of Hashin-
764 Shtrikman bounds based on Table 4 and on Bezacier *et al.* (2010) for glaucophane.
765 The bottom row lists values from Table 1 of Hacker *et al.* (2003b).

766

	tremolite	ferro-actinolite	hornblende	pargasite	tschermaktite	glaucophane	ferro glaucophane
Literature V_p km/s	7.1	6.3	7.20	7.3	6.7	7.6	7.0
V_s km/s	4.1	3.6	4.12	4.1	3.8	4.3	4.0
Poisson's ratio	.25	.26	.26	.27	.26	.26	.26
Density gm/cc	2.98	3.43	3.25	3.07	3.04	3.01	3.30
Current V_p km/s	7.4	6.5	7.22	7.7	7.6	7.5	
V_s km/s	4.5	3.8	4.21	4.5	4.5	4.6	
Poisson's ratio	.21	.27	.24	.23	.23	.20	
Density gm/cc	2.97	3.26	3.18	3.11	3.06	3.07	

767

768 Table 9. Isotropic compressional (V_p) and shear (V_s) velocities and densities for
769 selected amphiboles. Literature values are based on the compilation of Hacker *et al.*
770 (2003b). Current values are based on Table 5 for calcium amphiboles (using the
771 average calcium amphibole of Schumacher (2007) for hornblende) and Bezacier *et*
772 *al.* (2010) for glaucophane. Since hornblendite velocities were reported to four
773 significant figures by Christensen (1996) more precision is provided for the
774 hornblende table entries.